

Article

Effect of La₂O₃ as a Promoter on the Pt,Pd,Ni/MgO Catalyst in Dry Reforming of Methane Reaction

Ali M. A. Al-Najar¹, Faris A. J. Al-Doghachi^{1,*}, Ali A. A. Al-Riyahee¹ and Yun Hin Taufiq-Yap^{2,3,*}

¹ Department of Chemistry, Faculty of Science, University of Basrah, Basrah 61004, Iraq; aalnajar11@gmail.com (A.M.A.A.-N.); alriyaheea@yahoo.com (A.A.A.A.-R.)

² Chancellery Office, University Malaysia Sabah, Kota Kinabalu 88400, Sabah, Malaysia

³ Catalysis Science and Technology Research Centre, Faculty of Science, Universiti Putra Malaysia, Serdang 43400, Selangor, Malaysia

* Correspondence: farisj63@gmail.com (F.A.J.A.-D.); taufiq@upm.edu.my (Y.H.T.-Y.); Tel.: +96-478-0099-5900 (F.A.J.A.-D.); +60-397-696-809 (Y.H.T.-Y.)

Received: 8 April 2020; Accepted: 9 June 2020; Published: 6 July 2020



Abstract: Pt,Pd,Ni/MgO, Pt,Pd,Ni/Mg_{0.97}La³⁺_{0.03}O, Pt,Pd,Ni/Mg_{0.93}La³⁺_{0.07}O, and Pt,Pd,Ni/Mg_{0.85}La³⁺_{0.15}O (1% of each of the Ni, Pd, and Pt) catalysts were prepared by a surfactant-assisted co-precipitation method. Samples were characterized by the XRD, XPS, XRF, FT-IR, H₂-TPR, TEM, the Brunauer–Emmett–Teller (BET) method, and TGA and were tested for the dry reforming of methane (DRM). TEM and thermal gravimetric analysis (TGA) methods were used to analyze the carbon deposition on spent catalysts after 200 h at 900 °C. At a temperature of 900 °C and a 1:1 CH₄:CO₂ ratio, the tri-metallic Pt,Pd,Ni/Mg_{0.85}La³⁺_{0.15}O catalyst with a lanthanum promoter showed a higher conversion of CH₄ (85.01%) and CO₂ (98.97%) compared to the Ni,Pd,Pt/MgO catalysts in the whole temperature range. The selectivity of H₂/CO decreased in the following order: Pt,Pd,Ni/Mg_{0.85}La³⁺_{0.15}O > Pt,Pd,Ni/Mg_{0.93}La³⁺_{0.07}O > Pt,Pd,Ni/Mg_{0.97}La³⁺_{0.03}O > Ni,Pd,Pt/MgO. The results indicated that among the catalysts, the Pt,Pd,Ni/Mg_{0.85}La³⁺_{0.15}O catalyst exhibited the highest activity, making it the most suitable for the dry reforming of methane reaction.

Keywords: biogas; catalyst deactivation; dry reforming; H₂ production; Ni; Pd; Pt catalyst

1. Introduction

The dry reforming of methane (DRM) (Equation (1)) is a promising reaction for the simultaneous conversion of two major greenhouse gases (CO₂/CH₄) to syngas with an H₂/CO ratio of 1 and is thus suitable for the synthesis of oxygenated hydrocarbons and synthetic fuels [1]. Moreover, DRM can utilize biogas (mainly composed of CH₄ and CO₂) produced by the anaerobic fermentation of sludge waste as a renewable resource [2,3]. The main drawbacks of DRM are as follows: (1) the catalyst sintering at high temperature; (2) the occurrence of the reverse water–gas shift reaction (RWGS) (Equation (2)).



which lowers the H₂/CO ratio [4]; and (3) the fast catalyst deactivation due to carbon deposition from methane cracking (Equation (3)) and the Boudouard reaction (Equation (4)):



Catalysts containing noble metals, such as Pt, Ru, and Rh, show high activity and selectivity for the DRM reaction as well as good stability towards coke deposition; however, their high cost and low availability make them not economically competitive in comparison to other transition metal-based materials [5–7]. Among non-precious transition metals, cobalt and nickel supported on various oxide systems (MgO-ZrO₂, Al₂O₃, MgAl₂O₄, CeO₂, CeO₂-ZrO₂) showed promising performances. In particular, nickel has been reported as a very active metal for the DMR but was also reported to be highly prone to carbon formation [7,8]. Contradictory findings have been reported about cobalt [9,10]. Compared with nickel, cobalt generally showed better behavior towards the suppression of carbon deposition and better stability under reaction conditions [11].

Few studies have been reported on CeO₂ [8] and CeO₂-ZrO₂ [12]. For this reason, the objective of this study is to prepare a catalyst with a high activity, selectivity, stability, and ability to prevent carbon deposition on the catalyst during the dry reforming of methane reaction. The Pt,Pd,Ni/Mg_{1-x}La_xO catalysts are prepared using a co-precipitation method that uses K₂CO₃ as a precipitant, followed by the impregnation of 1% Pt, 1% Pd, and 1% Ni using Pt(acac)₂, Pd(acac)₂, and Ni(acac)₂, respectively. Subsequently, a study is conducted to compare the catalytic stability and coke formation. The study then investigates the effects of the concentrations of CO₂ and CH₄, the concentration of the catalysts, and the temperature of the conversion of the catalytic performance of the prepared catalysts in the dry reforming process, and it evaluates the stability of the catalysts.

2. Results and Discussion

2.1. Characterization of the Catalysts

2.1.1. XRD Patterns

Figure 1a–d reveals the XRD representations of the stimulants with MgO and La₂O₃ contents. Peak diffraction was observed at $2\theta = 36.9^\circ, 43.0^\circ, 62.8^\circ, 74.6^\circ, 78.6^\circ, \text{ and } 79.0^\circ$ due to the cubic shape of magnesia (JCPDS file No.: 00-001-1235). The peaks recorded at $2\theta = 25.3^\circ, 27.2^\circ, 30.2^\circ, 39.3^\circ, 54.7^\circ, \text{ and } 62.1^\circ$ were related to the cubic form of lanthanum oxide (JCPDS file No. 00-022-0369). The peaks ascribed to the cubic shape of the catalyst complex (Mg-La-O) were observed at $2\theta = 11.6^\circ, 15.4^\circ, 16^\circ, 28^\circ, 35.9^\circ, 46.9^\circ, 53.3^\circ, \text{ and } 68.2^\circ$. Similar findings and peak patterns were also reported by Grange [13]. On the other hand, no diffraction peaks were observed for Pt, Pd, and Ni due to their low concentration (less than 5%). The Debye–Scherrer equation was used to calculate the catalyst's crystal size. The crystal size was observed at 42.1, 44.7, 40.3, and 38.7 nm for the catalysts Pt,Pd,Ni/MgO, Pt,Pd,Ni/Mg_{0.97}La³⁺_{0.03}O, Pt,Pd,Ni/Mg_{0.93}La³⁺_{0.07}O, and Pt,Pd,Ni/Mg_{0.85}La³⁺_{0.15}O, respectively. The results show that the amount of lanthanum was inversely related to the crystal size whereby as the amount of lanthanum increased, the crystal size decreased. Moreover, this occurrence was due to the outgrowth of magnesia crystallites as a result of the effect of the residues of Pt, Pd, and Ni on the sample surface.

The XRD findings reveal a cubic crystal structure for all the samples. This result is backed by the TEM findings, which also show cubic shaped particles.

For the elemental analysis of all the components in the catalyst, X-ray fluorescence (XRF) was used. Table 1 shows the percentage of Ni, Pd, and Pt that were slightly more than 1 due to the incomplete precipitation of the Mg and La metal precursors in the method of co-precipitation. This had a slight effect on the results [4].

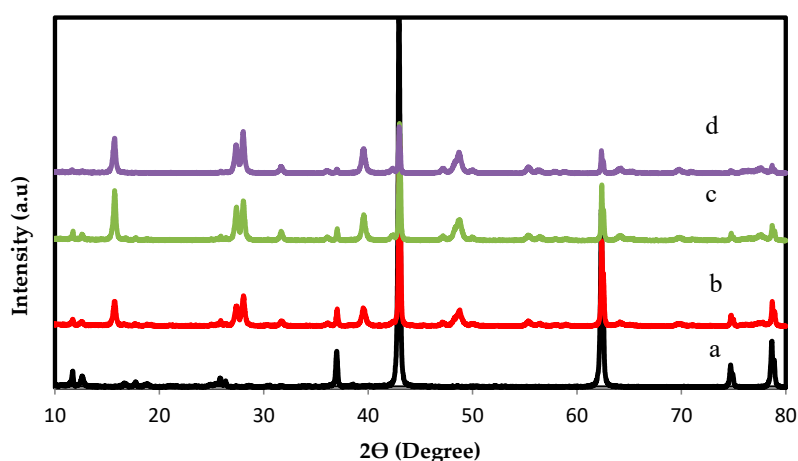


Figure 1. XRD patterns of the catalysts: (a) Pt,Pd,Ni/MgO, (b) Pd,Pd,Ni/Mg_{0.97}La³⁺_{0.03}O, (c) Pd,Pd,Ni/Mg_{0.93}La³⁺_{0.07}O, (d) Pd,Pd,Ni/Mg_{0.85}La³⁺_{0.15}O.

Table 1. Results of the particle size measurement by XRD, TEM, and XRF.

Catalysts	TEM (nm)	^a Crystal Size (D)		XRF		
		Debye–Scherrer Eq. (nm)	Ni%	Pd%	Pt%	Mg and La%
Pt,Pd,Ni/MgO	42.1	49	1.03	0.96	1.14	96.31
Pt,Pd,Ni/Mg _{0.97} La ³⁺ _{0.03} O ₃	44.6	66	0.95	1.05	0.93	95.93
Pt,Pd,Ni/Mg _{0.93} La ³⁺ _{0.07} O ₃	40.4	52	1.11	1.21	0.99	96.15
Pt,Pd,Ni/Mg _{0.85} La ³⁺ _{0.15} O ₃	38.6	50	1.14	0.98	1.09	96.56

^a Determined by the Debye–Scherrer equation of the Mg (200) plane of XRD.

2.1.2. FT-IR Spectra

Figure 2 shows the FT-IR data for all the catalysts (Pd,Pt,Ni/Mg_{0.97}La³⁺_{0.03}O, Pd,Pt,Ni/Mg_{0.93}La³⁺_{0.07}O, and Pd,Pt,Ni/Mg_{0.85}La³⁺_{0.15}O) that were prepared through the impregnation of Pt,Pd,Ni(acac)₂ on MgO-La₂O₃. The spectra of the unreduced catalysts showed bands in the region of 3616–893 cm⁻¹, which were assigned to the acetylacetonate part of the catalyst. The bands recorded at (1636–1579) cm⁻¹ and at (1420–1436) cm⁻¹ in the FT-IR were assigned to the C = O and C = C bonds, respectively, of acetylacetonate in the main catalyst Pt,Pd,Ni(acac)₂/MgO-La₂O₃ complexes. A band at around 3616–3659 cm⁻¹ was attributed to stretching frequency of moisture [14].

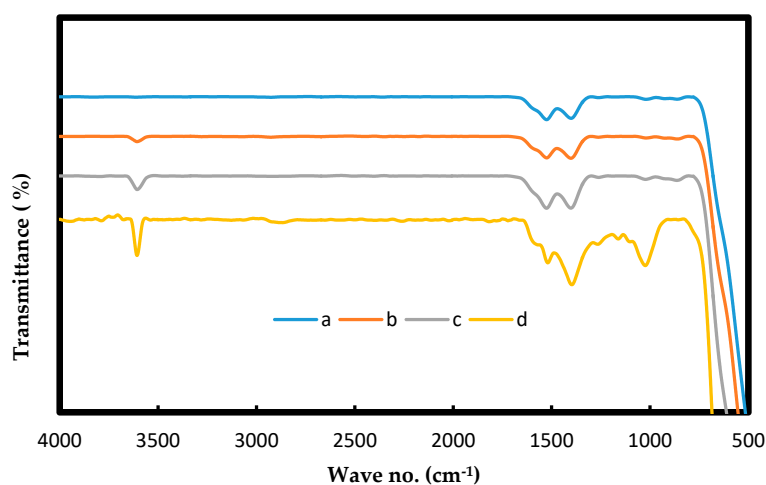


Figure 2. FT-IR spectra of the catalysts: (a) Pt,Pd,Ni/MgO, (b) Pd,Pd,Ni/Mg_{0.97}La³⁺_{0.03}O, (c) Pd,Pd,Ni/Mg_{0.93}La³⁺_{0.07}O, (d) Pd,Pd,Ni/Mg_{0.85}La³⁺_{0.15}O.

The bands for the metal oxides PtO and PdO were observed at 673 and 769 cm^{-1} , respectively, whereas the peaks for NiO, MgO, and LaO did not appear in the spectra due to their appearance at the far FT-IR range.

2.1.3. XPS Analysis

Figure 3a–d, shows the X-ray photoelectron spectroscopy (XPS) spectra of La3d, Mg2p, O1s, and Ni2p for the catalyst Pd,Pd,Ni/Mg_{0.85}La³⁺_{0.15}O. The XPS spectra detect metals on the surface of the catalyst (3–12 nm). Figure 3a provides an illustration of the spectra La3d of La₂O₃, with BE from 832 to 853.2 eV. The most thorough photoelectron indication is that of La-O, which is seen in the high BE area. Figure 3b interprets one significant peak gained from Mg2p, bulk Mg-O at a binding energy of 47.7 eV. Figure 3d exhibits five noticeable oxygen species for (O1s) that were observed at the top layer of the catalyst assigned to Ni-O, La-O, Mg-O, Pt-O, and Pd-O at binding energies of 527.4 and 529.2 eV. The binding energies of (Pt3d) and (Pd3d) were observed at 69.8 and at 1148.7 eV, respectively. Finally, the Ni2p spectra were observed at binding energies of 849.1 and 853.1 [15].

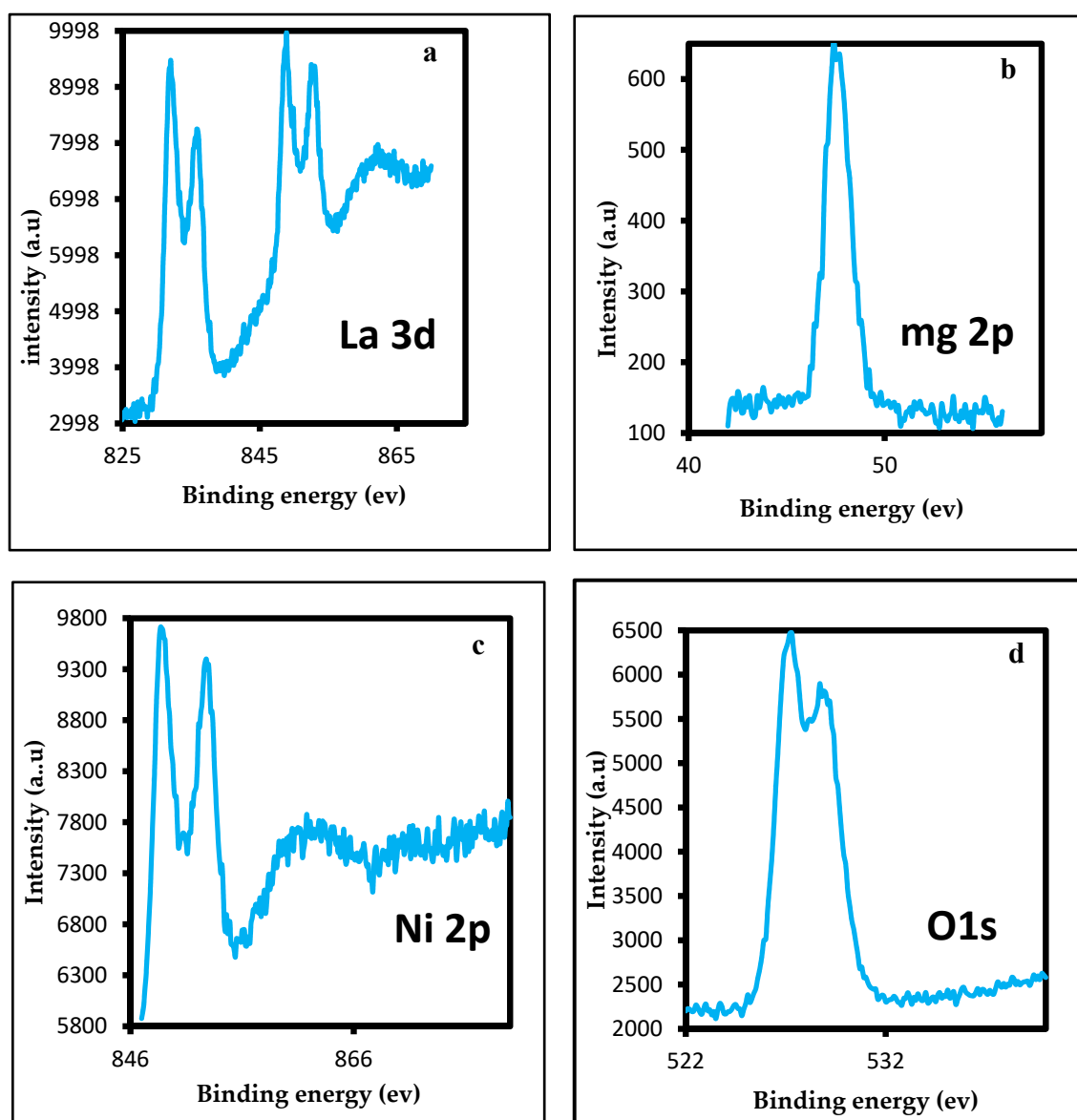


Figure 3. XPS narrow scans of the reduced catalyst: (a) La3d (b) Mg2p, (c) Ni2p, and (d) O1s.

2.1.4. Temperature Programmed Reduction (H₂-TPR)

H₂-TPR was used to characterize the reducibility of La₂O₃ for the reforming of the Pt,Pt,Ni catalysts. The H₂-TPR result for the Pt,Pt,Ni/Mg_{1-x}La³⁺_xO (where x = 0.00, 0.03, 0.07, 0.15) profiles is tabulated in Table 2, and the H₂-TPR patterns of the catalysts are illustrated in Figure 4. Figure 4a demonstrates three clearly defined reduction peaks in the TPR profile of the Pt,Pd,Ni/MgO. The first reduction peak appeared at 130 °C and was ascribed to the reduction of the PtO to Pt°. This finding differs from findings by Mahoney et al. [16], who identified the reduction of the PtO species to be at 114 °C. The second reduction peak was registered at 184 °C and occurred due to the reduction of PdO to Pd°. The third and final peak was recorded at a temperature of 621 °C and was attributed to the strong overlap of materials supporting the production of Ni, which concurs with findings by Bao et al. [17], where a reduction was observed in the NiO for the Ni/ZrMgAl catalyst at 516 °C. Figure 4b–d and Table 2 demonstrates the TPR profile for catalysts containing the La₂O₃ promoter. Five peaks were obtained by catalysts containing the La₂O₃ promoter, as can be seen in Figure 4b–d. The first three peaks of the Pt,Pd,Ni/Mg_{0.97}La³⁺_{0.03}O catalyst were recorded at 115, 175, and 573 °C while the peaks of the Pt,Pd,Ni/Mg_{0.93}La³⁺_{0.07}O were demonstrated at 123, 170, and 578 °C, and peaks of the Pt,Pd,Ni/Mg_{0.85}La³⁺_{0.15}O catalyst were seen at 126, 163, and 572 °C. This was due to a decrease in PtO, PdO, and NiO through the surface layer of the catalyst to gain the Pt°, Pd°, and Ni° elements, respectively. The fourth peak of the catalyst seen in Figure 4b–d was recorded at the temperatures of 532, 545, and 559 °C, respectively, and it was due to the presence of La₂O₃ on the surface. The fifth and final peak was observed at 635, 652, and 677 °C for the catalysts Pt,Pd,Ni/Mg_{0.97}La³⁺_{0.03}O, Pt,Pd,Ni/Mg_{0.93}La³⁺_{0.07}O, and Pt,Pd,Ni/Mg_{0.85}La³⁺_{0.15}O, respectively. The increase in temperature observed by the fifth peak was due to the strong reaction between the La₂O₃ promoter and the MgO support. When the load of the promoter La₂O₃ increased, the catalysts showed a high degree of reduction ability. This finding agrees with results obtained by previous studies, such as the study by Roberto et al. [18], who reported the reduction of lanthanum to occur at 490 and 790 °C.

Table 2. H₂-TPR values of the different catalysts.

Catalysts	Temp. °C	Amount of Adsorbed H ₂ Gas (μmol/g)				
Pt,Pd,Ni/MgO	130	184	621	-	-	464.8
Pt,Pd,Ni/Mg _{0.97} La ³⁺ _{0.03} O	115	175	573	532	635	503.7
Pt,Pd,Ni/Mg _{0.93} La ³⁺ _{0.07} O	123	170	578	545	652	515
Pt,Pd,Ni/Mg _{0.85} La ³⁺ _{0.15} O	126	163	572	559	677	572

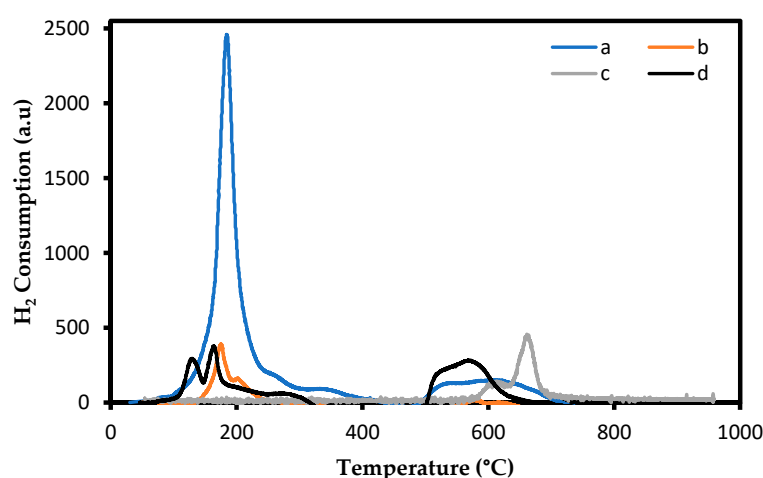


Figure 4. H₂-TPR profiles of the catalysts (a) Pt,Pd,Ni/MgO, (b) Pd,Pd,Ni/Mg_{0.97}La³⁺_{0.03}O, (c) Pd,Pd,Ni/Mg_{0.93}La³⁺_{0.07}O, and (d) Pd,Pd,Ni/Mg_{0.85}La³⁺_{0.15}O reduced in a (5% H₂/Ar) stream at a temperature ramp of 10 °C/min.

The total amount of H₂ consumed during the reduction process of the Pt,Pd,Ni/MgO, Pt,Pd,Ni/Mg_{0.97}La₂³⁺_{0.03}O, Pt,Pd,Ni/Mg_{0.93}La₃³⁺_{0.07}O, and Pt,Pd,Ni/Mg_{0.85}La₃³⁺_{0.15}O catalysts (Figure 4a–d) was calculated by the total peak area and was recorded at 464.8, 503.7, 515, and 572 μmol/g catalyst, respectively [13]. According to H₂-TPR results, the most active catalyst was Pt,Pd,Ni/Mg_{0.85}La₂³⁺_{0.15}O, suggesting its suitability for the DRM reaction.

2.1.5. Brunauer–Emmett–Teller (BET) Surface Area

The values of the specific surface area of BET (S_{BET}) and the pore properties of reduced catalyst supports for the Pt,Pd,Ni/Mg_{1-x}La_xO catalysts (where x = 0.00, 0.03, 0.07, and 0.15) are presented in Table 3. The Pt,Pd,Ni/MgO catalyst surface area was recorded at 12.97 m²/g, whereas the surface area of the support MgO was recorded at 11.1 m²/g. This difference was due to the effect of the Pt, Pd, and Ni loadings on the fixed surface area of the MgO support. On the other hand, the surface area of the Pt,Pd,Ni/MgO stimulant was lesser than the surface areas of the Pt,Pd,Ni/Mg_{0.97}La₂³⁺_{0.03}O, Pt,Pd,Ni/Mg_{0.93}La₃³⁺_{0.07}O, and Pt,Pd,Ni/Mg_{0.85}La₃³⁺_{0.15}O catalysts (b, c, and d), which were recorded at 13.79, 14.19, and 17.17 m²/g, respectively.

Table 3. The main textural properties of the fresh catalysts.

Sample Name	Specific Surface	Pore Volume	Pore Radius
	Area (m ² /g)	(cm ³ /g)	(Å)
MgO	11.1	0.21	9.9
Pt,Pd,Ni/MgO	12.97	0.12	9.7
Pt,Pd,Ni/Mg _{0.97} La ₃ ³⁺ _{0.03} O ₃	13.79	0.054	44.53
Pt,Pd,Ni/Mg _{0.93} La ₃ ³⁺ _{0.07} O ₃	14.19	0.082	30.87
Pt,Pd,Ni/Mg _{0.85} La ₃ ³⁺ _{0.15} O ₃	17.17	0.095	18.27

The pore volume of the Pt,Pd,Ni/Mg_{0.85}La₃³⁺_{0.15}O catalyst was 0.095 cm³/g and was higher than that of the Pt,Pd,Ni/Mg_{0.97}La₃³⁺_{0.03}O and Pt,Pd,Ni/Mg_{0.93}La₃³⁺_{0.07}O catalysts (0.054 and 0.082 cm³/g respectively).

Table 3 depicts the pore radius of different catalysts. The pore radius of the support MgO was 9.9 Å, whereas that of the Pt,Pd,Ni/MgO catalyst was 9.7 Å. The pore radius of the other catalysts and the rise of the La₂O₃ promoter in the support was inversely proportionate to one another. The pore radii of the catalysts (b, c, and d) were 44.53 Å, 30.87 Å, and 18.27 Å, respectively [19]. These data indicated that the Pt,Pd,Ni/Mg_{0.85}La₃³⁺_{0.15}O₃ catalyst with a high surface area recorded the best activity in the DRM reaction compared to other catalysts.

2.1.6. TEM Characterization

Figure 5a–d shows the distribution and morphology (shape and size) of the synthesized catalysts Pt,Pd,Ni/MgO, Pt,Pd,Ni/Mg_{0.97}La₃³⁺_{0.03}O, Pt,Pd,Ni/Mg_{0.93}La₃³⁺_{0.07}O, and Pt,Pd,Ni/Mg_{0.85}La₃³⁺_{0.15}O that were characterized by TEM and formed cubic structures. The catalysts underwent calcination at 1150 °C with a consistency in the distribution of particles without free La₂O₃. Figure 5b–d proves the formation of MgO-La₂O₃ solid solutions [20] with cubic oxide particles on the Pt, Pd, and Ni layers of the carrier metal. Each Pt,Pd,Ni/Mg_{0.85}La₃³⁺_{0.15}O catalyst (Figure 5d) dispersed 1% of the Pt, Pd, and Ni metal particles on the carrier MgO-La₂O₃ with sizes between 45 and 85 nm. On the other hand, the TEM analysis of the Pt,Pd,Ni/Mg_{0.85}La₃³⁺_{0.15}O catalyst reveals an induced growth with an agglomeration of the nanoparticles at a certain distance between the metal crystallites. It is necessary to pinpoint that this type of growth is often catalyzed by metallic platinum, palladium, and nickel, even although the distribution of the TEM image sizes is more realistic and accurate [21]. Hence, it is clear that Figure 5a–d exhibits TEM results that match the XRD data. To sum up, these findings disclose that Mg-La-O was not only complex but also cubic and identical to MgO and La₂O₃.

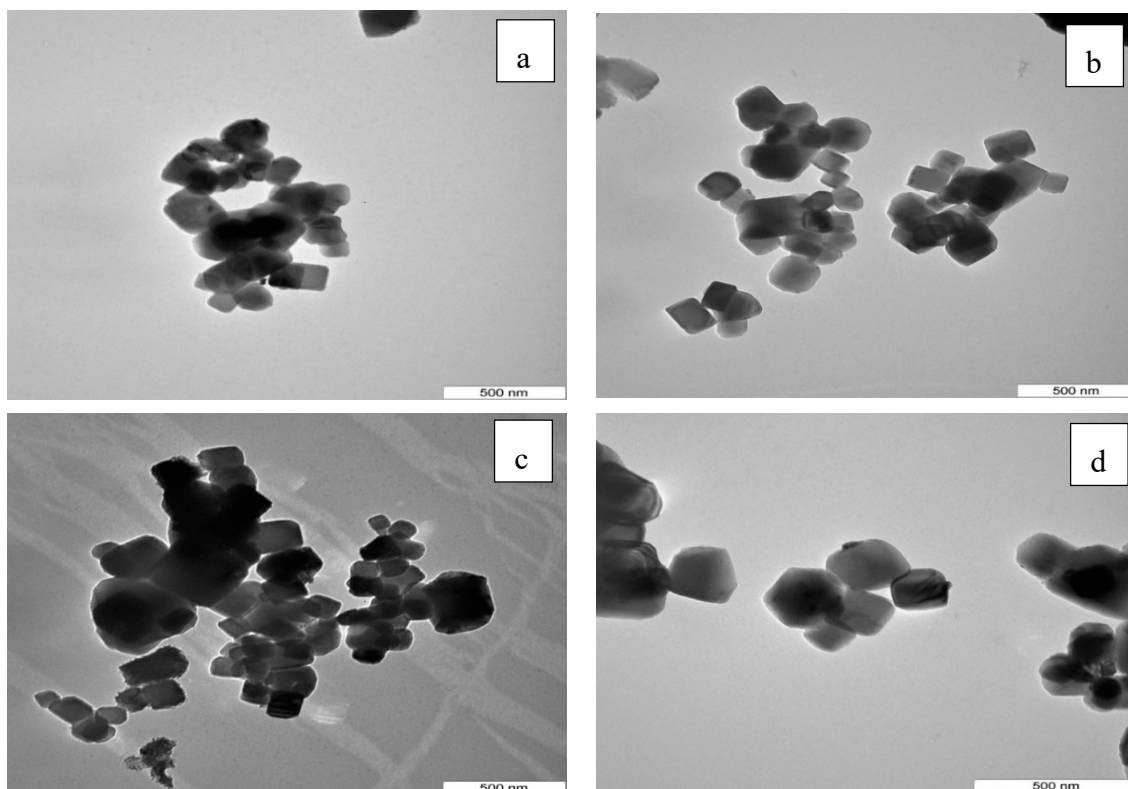


Figure 5. TEM images of catalysts: (a) Pt,Pd,Ni/MgO, (b) Pt,Pd,Ni/Mg_{0.97}La³⁺_{0.03}O, (c) Pt,Pd,Ni/Mg_{0.93}La³⁺_{0.07}O, (d) Pt,Pd,Ni/Mg_{0.85}La³⁺_{0.15}O.

2.1.7. Thermal Analysis

Figure 6a–d displays the TGA results for the Pt,Pd,Ni/MgO, Pt,Pd,Ni/Mg_{0.97}La³⁺_{0.03}O, Pt,Pd,Ni/Mg_{0.93}La³⁺_{0.07}O, and Pt,Pd,Ni/Mg_{0.85}La³⁺_{0.15}O catalysts. The initial findings show that there was an insignificant rise in the total weight of the compound owing to the mixture of N₂ gas in the device, which adsorbed to the surface of the catalysts. It is necessary to mention that the findings revealed that the weight loss process happened in only one stage of the Pt,Pd,Ni/MgO catalyst. The peak lost about 4% of the compound due to the loss of moisture at 100–120 °C. The other catalysts showed three peaks, in which the first was observed at 100–150 °C, which demonstrated a 5.2%, 6.3%, and 7.1% weight loss due to the loss of moisture. The second peak was due to a weight loss of 4.5% by Pt,Pd,Ni/Mg_{0.97}La³⁺_{0.03}O, 5.0% by Pt,Pd,Ni/Mg_{0.93}La³⁺_{0.07}O, and 5.2% by Pt,Pd,Ni/Mg_{0.85}La³⁺_{0.15}O at a temperature of 250 °C (see Figure 6c,d). Finally, the third peak appeared at 425 °C with a weight loss of 5.5%, 5.7%, and 5.9% for the Pt,Pd,Ni/Mg_{0.97}La³⁺_{0.03}O, Pt,Pd,Ni/Mg_{0.93}La³⁺_{0.07}O, and Pt,Pd,Ni/Mg_{0.85}La³⁺_{0.15}O catalysts, respectively, due to the loss of oxygen atoms from the catalyst. All the compounds were maintained stable at 650 °C. For the most part, this stability was due to the high melting point of magnesia and La₂O₃ at 2852 and 2315 °C, respectively. As to Figure 6a–d, the components of the catalyst reacted well with one another as supported by findings by Mojovic et al. [22].

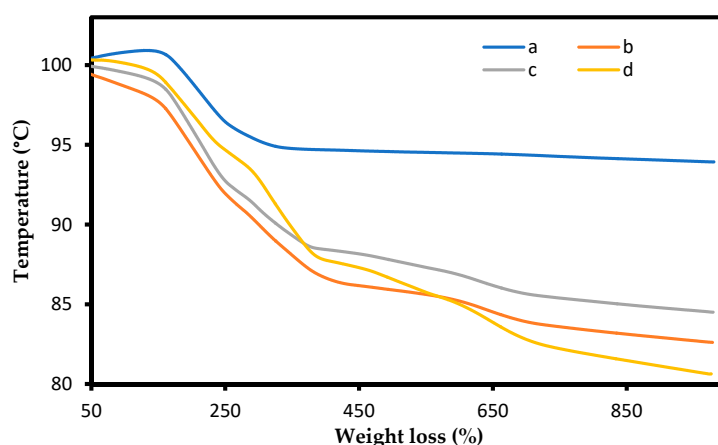


Figure 6. TG of the catalysts: (a) Pt,Pd,Ni/MgO, (b) Pt,Pd,Ni/Mg_{0.97}La³⁺_{0.03}O, (c) Pt,Pd,Ni/Mg_{0.93}La³⁺_{0.07}O, (d) Pt,Pd,Ni/Mg_{0.85}La³⁺_{0.15}O.

2.2. Catalytic Performance in Biogas Reforming

2.2.1. Effects of Reactant Concentration on Conversion

The reaction activity of DRM was demonstrated by the conversion of CH₄ and CO₂ gas. The H₂/CO ratio shows the selectivity and the main test results without using the catalyst in which the presence of H₂ and CO was observed in the outgas at a temperature of more than 900 °C due to the decomposition of methane in Equation (3). Then, when the metals were not used in the catalyst Mg_{1-x}La_xO, the conversion of CH₄ and CO₂ was very low and insignificant with a recording of 36% and 50%, respectively, and an H₂/CO ratio of 0.3 at a reactant ratio (CH₄:CO₂) of 1:1. On the other hand, at a 1:2 ratio, the results of methane and carbon dioxide conversion were 24% and 43%, respectively. As for the H₂/CO ratio, it was 0.12 as shown in Figure 7. These findings reveal the presence of a poor interaction in the pores of the supportive promoter, which is in line with the BET results that show the presence of pores in the catalyst. When the catalysts Pt,Pd,Ni/Mg_{1-x}La³⁺_xO were used (Figure 8), a rise in the conversion of CH₄ (85.01%) and CO₂ (98.97%) and the H₂/CO (1.15) ratio was observed, indicating that Pt, Pd, and Ni metals loading on the support have a significant effect in the catalytic reaction of Pt,Pd,Ni/Mg_{0.85}La³⁺_{0.15}O. At a reactant ratio of 1:2, the CH₄ and CO₂ conversions were 80.8% and 94%, respectively, and the H₂:CO ratio was 1.07. These results reveal that the 1:1 ratio was the most effective ratio in opposing the deactivation of the catalyst due to carbon deposition and resulted in a higher selectivity of H₂ and CO (Figure 8). Similar observations were noted by the other catalysts [23].

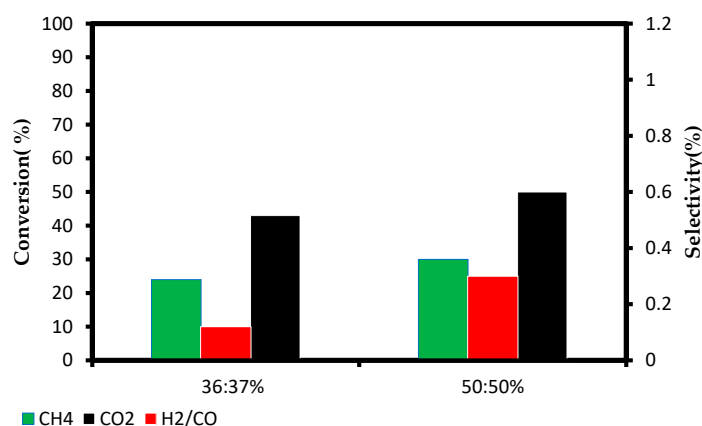


Figure 7. The effect of changing the ratio concentration of the CH₄:CO₂ reactant a—(2:1) and b—(1:1) over the percentage of their conversion and H₂/CO ratio for the support-promoter (Mg_{1-x}La_xO) of the catalyst at 900 °C.

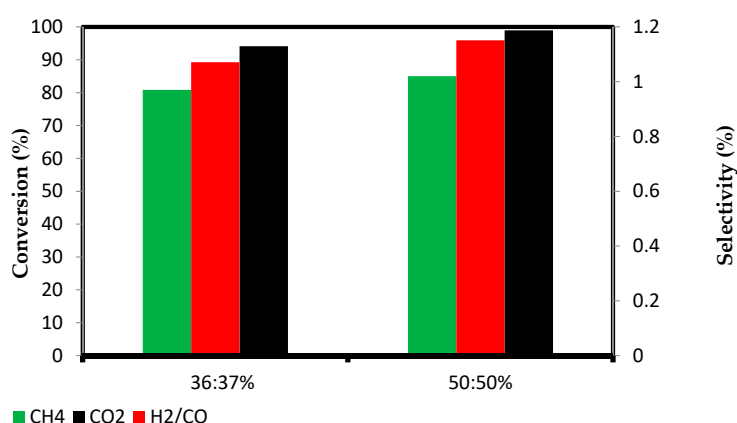


Figure 8. The effect of changing the ratio concentration of the CH₄:CO₂ reactant a—(2:1) and b—(1:1) over the percentage of their conversion and H₂/CO ratio for Pt,Pd,Ni/Mg_{0.85}La³⁺_{0.15}O catalyst at 900 °C.

2.2.2. Effects of Concentration of the Catalyst on Conversion

Figure 9 and Table 4 show the effect of using different catalyst concentrations through the conversion process. The reaction conditions were set at 900 °C and 1 atm with a 1:1 reactant ratio (CH₄:CO₂). The conversion of CH₄, CO₂, and the H₂/CO ratio reveal that the catalysts were coordinated in the following arrangement: Pt,Pd,Ni/MgO < Pt,Pd,Ni/Mg_{0.97}La³⁺_{0.03}O < Pt,Pd,Ni/Mg_{0.93}La³⁺_{0.07}O < Pt,Pd,Ni/Mg_{0.85}La³⁺_{0.15}O. The highest reading of methane conversion was recorded for the Pt,Pd,Ni/Mg_{0.85}La³⁺_{0.15}O catalyst (85%), whereas the lowest reading was recorded for the Pt,Pd,Ni/MgO catalyst (72.83%).

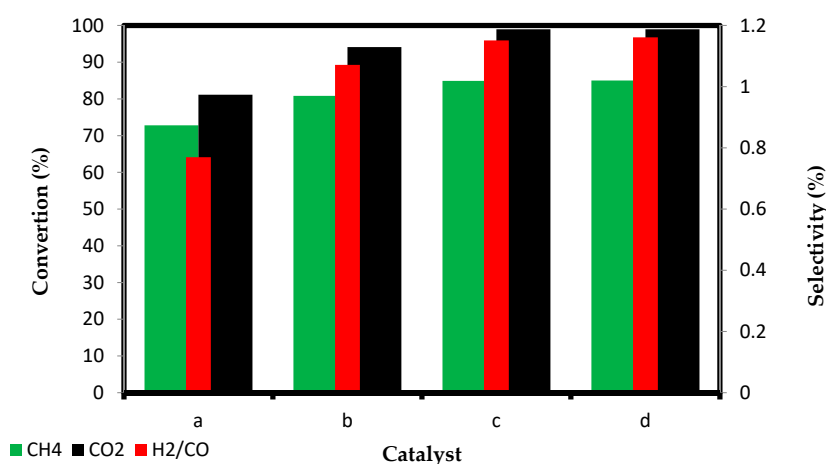


Figure 9. The effect of using different catalysts (a) Pt,Pd,Ni/MgO, (b) Pt,Pd,Ni/Mg_{0.97}La³⁺_{0.03}O, (c) Pt,Pd,Ni/Mg_{0.93}La³⁺_{0.07}O, and (d) Pt,Pd,Ni/Mg_{0.85}La³⁺_{0.15}O on CH₄, CO₂ conversion, and H₂/CO ratio at 900 °C for the 1:1 ratio of CH₄:CO₂.

Table 4. The catalytic results of DRM reaction for the catalysts at 900 °C for the 1:1 ratio of CH₄:CO₂.

Catalyst	CH ₄	CO ₂	H ₂ /CO
	Conversion %	Conversion %	Conversion %
Mg _{1-x} La _x O	36	50	0.3
Pt,Pd,Ni/MgO	72.83	81.14	0.7
Pt,Pd,Ni/Mg _{0.97} La ³⁺ _{0.03} O	80.86	94.17	1.07
Pt,Pd,Ni/Mg _{0.93} La ³⁺ _{0.07} O	84.92	98.96	1.15
Pt,Pd,Ni/Mg _{0.85} La ³⁺ _{0.15} O	85.01	98.97	1.16

The recorded CH₄ conversion was less stable than the CO₂ conversion. For the CO₂ conversion process, the catalyst Pt,Pd,Ni/Mg_{0.85}La³⁺_{0.15}O demonstrated a higher conversion rate (98.97%) when compared to the catalyst Pt,Pd,Ni/MgO, which demonstrated a CO₂ conversion rate of 81.14%. The findings made it clear that the most effective conversion process was observed by the catalyst Pt,Pd,Ni/Mg_{0.85}La³⁺_{0.15}O. The catalyst's H₂/CO ratio was higher than 1 (Figure 9 and Table 4). Such findings reveal that the process of CO₂ conversion of Ni metal showed less suitable findings than that of the tri-metallic catalysts, which is supported by a previous study [16].

Table 4 makes it evident that the rise in the CH₄, CO₂ conversion and the ratio of H₂/CO occurred due to the increase in the concentration of La₂O₃. This finding implies that the best results were observed by Pt,Pd,Ni/Mg_{0.85}La³⁺_{0.15}O catalyst as it had the largest surface area, as shown by the BET method (17.17 m²/g), and the largest active site as shown by the H₂-TPR (572 μmol/g) (Tables 2 and 3). This incident shows that the addition of La₂O₃ into the MgO catalysts can significantly lessen the reverse water–gas shift (RWGS) reaction (Equation (2)).

In addition, the findings demonstrate that the strong interference between the La₂O₃ promoter and the MgO support in the solid solution affects the CO formation rate in the DRM reaction. In such a way, the active site production process is vital for the CO₂ reforming of methane. The existence of the complete La₂O₃ promoter as a solid solution led the two oxides to become stable. When hydrogen was slashed at 700 °C, only the surface layer of the La₂O₃ solid solution of the La₂O₃-MgO catalyst was shrunk.

Moreover, the increase in the active sites as a result of an increase in La₂O₃ was ascribed to a good interaction between the Pt, Pd, and Ni particles and MgO-La₂O₃. When the Pt, Pd, and Ni concentrations in the carrier increased, the CH₄ and CO₂ conversion and selectivity showed no significant change. This may have occurred due to the formation of XRD nanoparticles (see Debye–Sherrer's equation and TEM results in Table 1). Although the X-ray diffraction was used for a simplified and possible estimate of the crystal size from the expansion of XRD reflections using the Scherrer formula, nanoparticles were preferred for molecules.

It could be noted that the selected nanoparticles as catalysts for this study raised the surface area and involved more reactions. These catalysts allowed Pt, Pd, and Ni to effectively disperse metals on the surface of the catalyst and furnished Lewis's strong fundamentals with metal oxide trusses. Moreover, increasing Lewis's primary support enhanced the catalyst's capacity to take in carbon dioxide in the DRM reaction. The formation of carbon dioxide occurred when the adsorbed carbon dioxide reacted with the deposited carbon (Equation (5)) with a lower coke formation.



2.2.3. Effects of Temperature on Conversion

Figure 10 sheds light on the selectivity and activity of the Pd,Pd,Ni/Mg_{0.85}La³⁺_{0.15}O catalyst from 700 to 900 °C. The CH₄:CO₂ (1:1) conversion increased when the temperature was increased from 700 to 900 °C due to the endothermic DRM reaction. In addition, the rise in temperature in the conversion rate contributed to the increase in the conversion rate of CH₄ and CO₂. This occurrence has been reported in previous studies [24]. As the temperature rose from 700 to 900 °C, the CH₄ conversion of Pd,Pd,Ni/Mg_{0.85}La³⁺_{0.15}O increased from 32.67% to 85% C, whereas the CO₂ conversion increased from 36.63% to 98.97%.

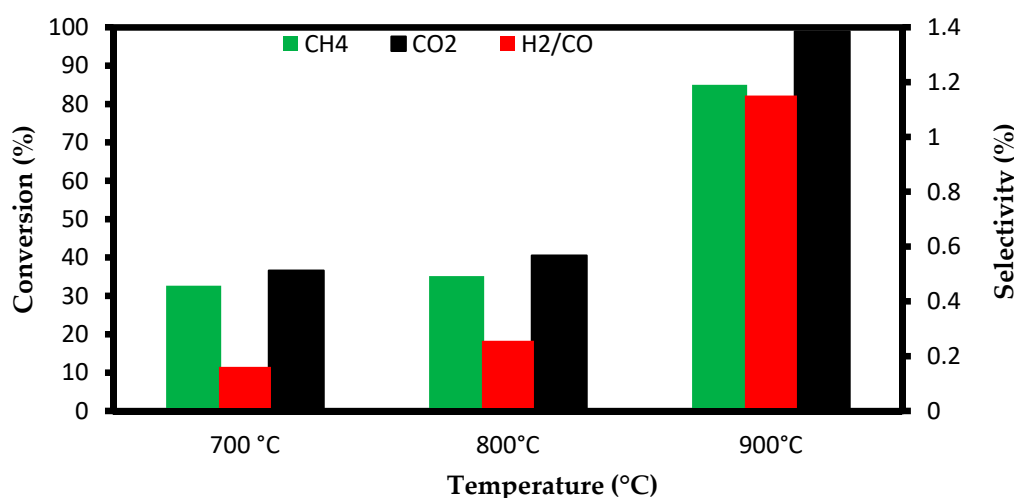
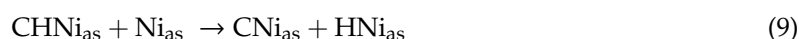


Figure 10. The influence of temperature on the catalytic activity of the Pd,Pd,Ni/Mg_{0.85}La³⁺_{0.15}O catalyst: (1) 700 °C, (2) 800 °C, (3) 900 °C for the 1:1 ratio of CH₄:CO₂.

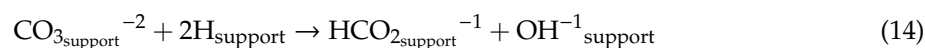
There was no significant increase in the CH₄ and CO₂ conversions at temperatures above 900 °C. Figure 9 sheds light on the H₂/CO ratio of the catalyst at different temperatures. When the temperature was higher than 900 °C, the H₂/CO ratio of the catalyst was less than 1. At a temperature of 900 °C, the H₂/CO ratio of Pd,Pd,Ni/Mg_{0.85}La³⁺_{0.15}O catalyst was 1.16 due to the minimal effect of (RWGS) reaction in Equation (2) [25].

2.2.4. Stability Tests

Figure 11 reveals that at a temperature of 900 °C, a high rate of methane and CO₂ diffusion was achieved. Firstly, methane was adsorbed on the nickel surface of the catalyst to produce hydrogen, leading to the formation of carbon on the surface of nickel as shown by the following mechanism (Equations (6)–(10)):



where (as) indicates active site. Secondly, the CO₂ accumulated on the promoter (La₂O₃) to produce CO and O (Equations (11)–(15)):



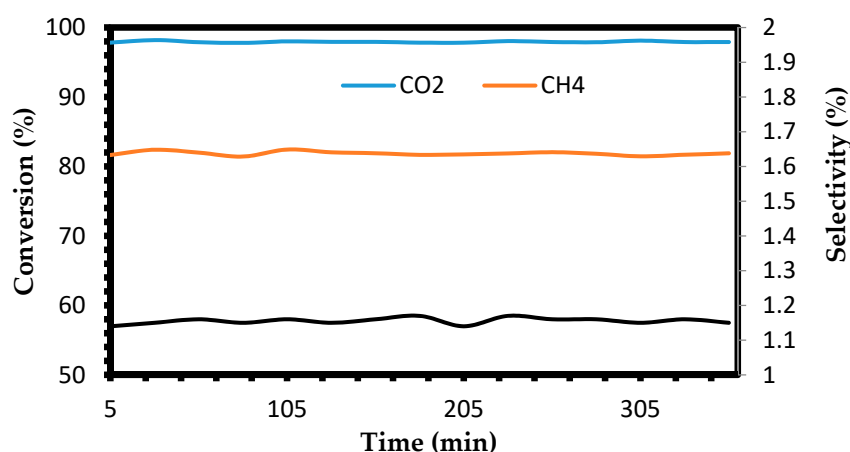


Figure 11. Stability tests of the Pt,Pd,Ni/Mg_{0.85}La³⁺_{0.15}O catalysts at 900 °C for the 1:1 ratio of CH₄:CO₂, for 200 h (GHSV = 15,000 mL·cat⁻¹·h⁻¹, atmospheric pressure).

The accumulation of carbon on the surface of the metal is known to curb the stability of the catalyst, which is counteracted by the availability of the La₂O₃ promoter that helps get rid of the deposited carbon and reactivates the catalyst. The main factor for the continuation of the reaction for 200 h or more was the usage of the La₂O₃ promoter in the catalyst, which ensured a very stable platform and a strong coke resistance. The carbon that was formed on the catalyst during the DRM reaction was removed by La₂O₃. This phenomenon was followed by the formation of carbonate types, especially La₂O₃, which can change carbon dioxide into CO and O. Finally, an O atom was generated with C that was deposited on the Ni metal catalyst to produce CO [26]. Based on the results, a significant decrease in the deposition of carbon on the catalyst was observed (Equations (16) and (17)):



All in all, significant changes occurred in the surface properties of both metal oxides [27] because lanthanum is an oxide with a proven capacity to strongly react during the metal carrier phase. The activity and persistence of the Pt, Pd, and Ni catalysts had better results than Ni or the Pd-Ni polymetallic catalysts and bimetallic Pt-Ni catalysts. Undoubtedly, this may have occurred as a result of the transfer of the electron density from Pd and Pt to Ni (the main catalyst) in the three-metal catalyst, as indicated in our previous work. To sum up, this result is consistent with the hypothesis that Pt and Pd can prevent nickel oxidation while increasing the electron density [28,29].

2.2.5. Post-Reaction Characterization

The TGA and TEM images show a very small consolidation of coke deposits from the spent catalyst. Figure 12 shows TEM images of spent catalysts in which a similar structure of the catalyst was intact even after being subjected to a current test for 6 h. In addition, there was no change in the two-dimensional cube texture of the spent catalyst. The TEM results show stratified carbon deposition with no filamentous carbon effect. As for Figure 13, the TGA with oxygen flow was provided by the posterior reaction of the catalyst Pt,Pd,Ni/Mg_{0.85}La³⁺_{0.15}O and a weight change calculation for each temperature range with reference to the thermo-couple. Moreover, it was noted that there were three different regions with different temperature ranges in which the first range was small due to the increased weight of the catalyst used. The second range was in the medium range, due to the lowering in the weight of the catalyst. The third range was observed in the high range (673 °C), owing to the elevated weight of the used catalyst (1.6%). The rise in weight was caused by the oxidation of the nickel,

platinum, and palladium particles at temperatures exceeding 100 °C. On the other hand, Chu et al. [30] reported that the weight gain of the spent catalyst was lower than 3%.

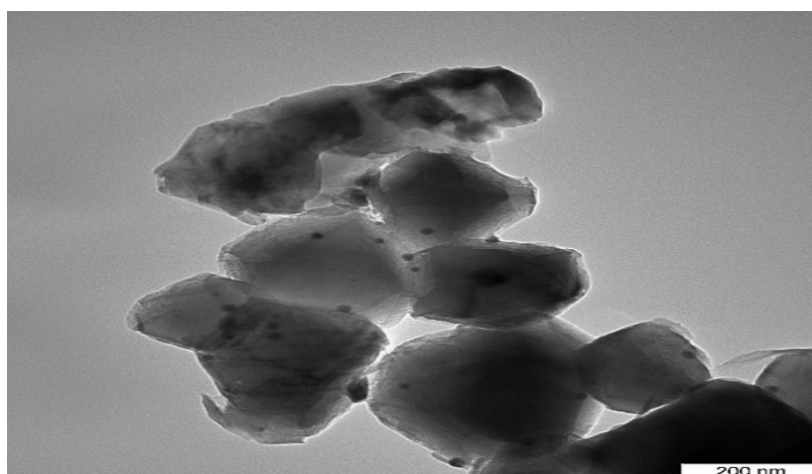


Figure 12. TEM analysis of the spent Pt,Pd,Ni/Mg_{0.85}La³⁺_{0.15}O catalyst after reaction: at 900 °C, and CH₄:CO₂ ratio 1:1.

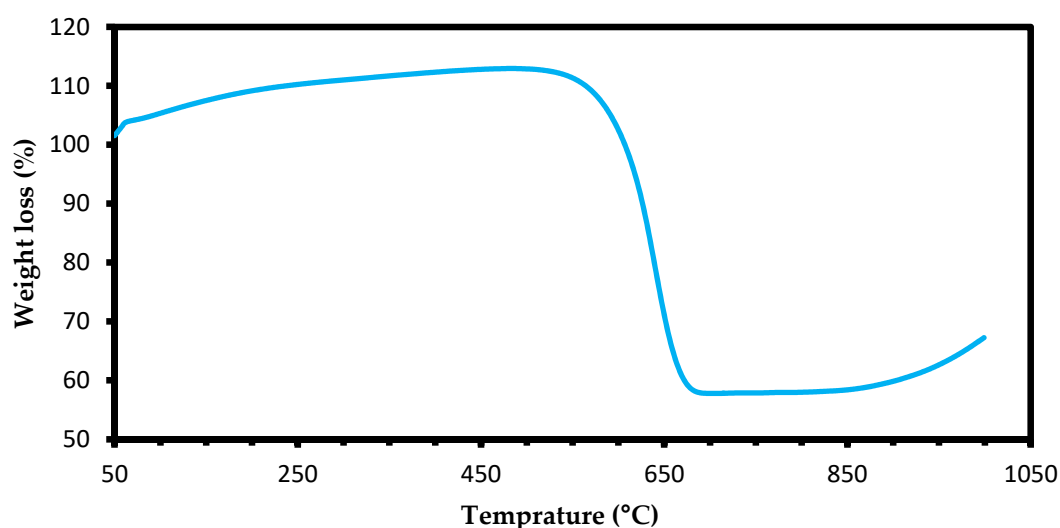


Figure 13. TGA profiles of the spent Pt,Pd,Ni/Mg_{0.85}La³⁺_{0.15}O catalyst (20 mL/min O₂ stream under a temperature ramp of 10 °C/min).

3. Experimental Section

3.1. Materials

La(NO₃)₃·6H₂O (99.0%), Mg(NO₃)₂·6H₂O (99.0%), and K₂CO₃ (99.7%) were obtained from the Merck company (Kenilworth, NJ, United States). Pt(C₅H₇O₂)₂·H₂O (99.0%) and Ni(C₅H₇O₂)₂·H₂O (99.0%) were supplied by Acros Organics (Waltham, MA., United States), while Pd(C₅H₇O₂)₂·H₂O (99.5%) was obtained from the Sigma-Aldrich company (St. Louis, MO, United States).

3.2. Preparation of Catalysts

The co-precipitation method was used for the preparation of the catalysts Mg_{1-x}La_xO (x = 0.00, 0.03, 0.07, and 0.15). The support of MgO and the promoter lanthanum oxide of La₂O₃ were prepared according to the methods used in [31] by using a (0.1) M La(NO₃)₃·6H₂O Mg(NO₃)₂·6H₂O and (1.0 M) K₂CO₃. Firstly, the sample was washed in warm water after the filtration of the precipitant. Next,

the sample was dried at 120 °C for 12h, following which the precipitant was pre-calcined in the air at 500 °C for 5 h to remove the CO₂. The sample was then pressed into discs at 600 kg/m². Finally, the sample was calcined at 1150 °C for 20 h to improve the mechanical properties and to ensure a smooth interaction between MgO and La₂O₃. Table 1 lists the steps involved in preparing the Pt,Pd,Ni(acac)₂/Mg_{1-x}La_xO catalysts (1%) concentrations of each Ni, Pd, and Pt metals. First, Pt(C₅H₇O₂)₂·H₂O was used to impregnate the 1% Pt dissolved in dichloromethane for 5 h to produce Pt(acac)₂/Mg_{1-x}La_xO. Then, the catalyst was impregnated with (1%) of Pd and Ni each. Pd(C₅H₇O₂)₂ and Ni(C₅H₇O₂)₂·H₂O solutions in dichloromethane were used for 5 h for the preparation of the catalysts. The catalysts were dried at 120 °C for 12 h after impregnation in the air. Finally, the catalysts were grinded and sieved into particles of sizes 80–150 or 150–250 µm in diameter.

3.3. Characterization of the Catalysts

A X-ray diffractometer (Shimadzu model XRD-6000, Nishinokyo, Kanda-nishiki-cho 1-chome Chiyoda-ku, Tokyo, Japan) was adopted in this study. X-ray photoelectron spectroscopy (XPS) results were acquired using the Kratos Axis Ultra DLD system (Kratos Analytical Limited, Trafford Park, MCR, UK) fixed with a monochromatic Al K α (1486.6 eV) and two X-ray sources (Al and Mg). The operation of the X-ray gun, which is the source of excitation, was conducted on an emission current of 20 mA combined with 15 kV voltages (Kratos Analytical Limited, Trafford Park, MCR, UK). The mode of operation for this hemispherical analyzer relied on fixed analyzer transmission (FAT) for wide and narrow scanning. The size of the pass energy was fixed at 100 and 40 eV. The region of interest for the narrow scan and photoelectron signals O1s, Mg2p, La3d, Ni2d, Pd3d, and Pt4f conformed to each other. The carbon charging correction referred to the binding energy of 285 eV for adventitious carbon. The radiation process occurred in a Philips glass diffraction X-ray tube of broad focus at 2.7 kW. The size of the crystals was calculated using the Debye–Scherrer relationship [32]. The assessment of the catalyst's active site was carried out through adopting the temperature programmed reduction (H₂-TPR) method that required hydrogen (Thermo Fisher Scientific, Waltham, MA, USA).

The apparatus that was used to set out the assessment was the Thermo Finnegan TPDRO 1100, accompanied by a thermal conductivity detector (Santa Clara, CA, USA). The total surface area of the catalyst was measured using the Brunauer–Emmett–Teller (BET) method with nitrogen adsorption set at –196 °C (Thermo Fisher Scientific, Waltham, MA, USA). Meanwhile, the Thermo Fisher Scientific S.P.A (model: Surfer Analyzer, Thermo Fisher Scientific, Rodano, MI, Italy) nitrogen adsorption-desorption analyzer was adopted for analysis. An apparatus for transmission electron microscopy (TEM) (Hitachi H7100 TEM with an increasing voltage of 10 MV, Chiyoda, Tokyo, Japan) was used to diagnose the crystal system and the catalyst's homogeneity.

In essence, to carry out the thermo-gravimetric analysis (TGA), the apparatus Mettler Toledo TG-DTA (Pt crucibles, Pt/Pt-Rh thermo-couple, Mettler-Toledo, Shah Alam, SGR, Malaysia) and a heating range of 50 to 1000 °C were applied.

3.4. Catalytic Evaluations

The production of syngas (H₂/CO) as the model for the reforming of biogas was conducted using a fixed bed stainless steel micro-reactor (i.d. \varnothing = 6 mm, h = 34 cm) during the catalytic evaluation for DRM. A mass flow gas controller (SIERRA instruments, Monterey, CA, USA) and an online gas chromatography (GC) (Agilent 6890N; G 1540N, Santa Clara, CA, USA) equipped with Varian capillary columns HPPLLOT/Q and HP-MOLSIV were connected to a reactor. Before the start of the process, a reduction of approximately 0.02 g of the catalyst was conducted by flowing 5% H₂/Ar at 700 °C, and the holding period was 3 h. The aim of the reduction step was to convert the (Ni²⁺, Pd²⁺, and Pt²⁺) phase of the catalyst to the metal (Ni, Pd, and Pt) phase at the active sites of the catalysts. The tested catalyst was held in a vertical position using plugs of quartz wool in the middle of a reactor. A thermo-couple was placed into the catalyst chamber to control and check the reaction temperature.

The calculations of the conversions for CH₄ and CO₂, the selectivity for H₂ and CO, as well as ratios for syngas (H₂/CO), are based on Equations (18)–(22):

$$\text{CH}_4 \text{ Conversion \%} = \frac{(\text{CH}_4)_{\text{in}} - (\text{CH}_4)_{\text{out}}}{(\text{CH}_4)_{\text{in}}} * 100 \quad (18)$$

$$\text{CO}_2 \text{ Conversion \%} = \frac{(\text{CO}_2)_{\text{in}} - (\text{CO}_2)_{\text{out}}}{(\text{CO}_2)_{\text{in}}} * 100 \quad (19)$$

$$\text{H}_2 \text{ Selectivity \%} = \frac{(\text{H}_2)}{2[(\text{CH}_4)_{\text{in}} - (\text{CH}_4)_{\text{out}}]} * 100 \quad (20)$$

$$\text{CO Selectivity \%} = \frac{(\text{CO})}{2[(\text{CH}_4)_{\text{in}} - (\text{CH}_4)_{\text{out}}] + [(\text{CH}_4)_{\text{in}} - (\text{CH}_4)_{\text{out}}]} * 100 \quad (21)$$

$$\text{H}_2/\text{CO ratio} = \frac{\text{H}_2 \text{ Selectivity \%}}{\text{CO Selectivity \%}} \quad (22)$$

4. Conclusions

The dry reforming of methane over the Pt,Pd,Ni/Mg_{1-x}La_xO catalysts was carried out for the production of syngas. The catalysts were synthesized using the co-precipitation method with K₂CO₃ as the precipitant and were characterized for their physico-chemical properties by XRD, XPS, XRF, H₂-TPR, BET, TEM, and TGA methods. The results demonstrated that at a temperature of 900 °C and H₂/CO and CH₄: CO₂ ratios of 1.16 and 1:1, respectively, the Pt,Pd,Ni/Mg_{0.85}La₂³⁺_{0.15}O catalyst exhibited the highest activity and stability, resulting in favorable CO₂ and CH₄ conversion rates of 98.97% and 85.01%, respectively. The different results of the catalysts showed that the catalytic performances of the catalysts strongly depended on the nature and concentration of the promoter. Finally, the stability of the Pt,Pd,Ni/Mg_{0.85}La₂³⁺_{0.15}O catalyst was investigated for 200 h and showed a very minor carbon formation, indicating that the catalyst was resistant to carbon formation.

Author Contributions: Conceptualization, A.M.A.A.-N., F.A.J.A.-D., A.A.A.A.-R. and Y.H.T.-Y.; methodology, A.M.A.A.-N., F.A.J.A.-D. and Y.H.T.-Y.; software, A.M.A.A.-N. and F.A.J.A.-D.; validation, A.M.A.A.-N., F.A.J.A.-D. and Y.H.T.-Y.; formal analysis, A.M.A.A.-N. and F.A.J.A.-D.; investigation, A.M.A.A.-N., F.A.J.A.-D.; resources, F.A.J.A.-D. and Y.H.T.-Y.; data curation, A.M.A.A.-N. and F.A.J.A.-D.; writing—original draft preparation A.M.A.A.-N. and F.A.J.A.-D.; writing—review and editing, A.M.A.A.-N., F.A.J.A.-D. and A.A.A.A.-R.; visualization, A.M.A.A.-N., F.A.J.A.-D. and Y.H.T.-Y.; supervision, F.A.J.A.-D., A.A.A.A.-R. and Y.H.T.-Y.; project administration, F.A.J.A.-D., A.A.A.A.-R. and Y.H.T.-Y.; funding acquisition, F.A.J.A.-D., Y.H.T.-Y. All authors have read and agreed to the published version of the manuscript.

Funding: The authors thank the NanoMite Grant (Vot. No: 5526308) for the provision of the necessary funds to carry out this study.

Acknowledgments: The authors would like to thank the PUTRACAT lab for permission to use the lab.

Conflicts of Interest: The authors declare no conflict of interest.

References

- Jiang, Z.; Xiao, T.; Kuznetsov, V.L.; Edwards, P.P. Turning carbon dioxide into fuel. *Philos. Trans. R. Soc. A* **2010**, *368*, 3346–3364. [[CrossRef](#)] [[PubMed](#)]
- Chandra, R.; Takeuchi, H.; Hasegawa, T. Methane production from lignocellulose agricultural crop wastes: A review in context to second generation of biofuel production. *Renew. Sustain. Energy Rev.* **2012**, *16*, 1462–1476. [[CrossRef](#)]
- Demirbas, M.F.; Balat, M.; Balat, H. Biowastes to biofuels. *Energy Convers. Manag.* **2011**, *52*, 1815–1828. [[CrossRef](#)]
- Oyama, S.T.; Hacıoğlu, P.; Gu, Y.; Lee, D. Dry reforming of methane has no future for hydrogen Hydrogen production: Comparison with steam reforming at high pressure in standard and membrane reactors. *Int. J. Energy* **2012**, *37*, 10444–10450. [[CrossRef](#)]

5. Djinovic, P.; Batista, J.; Pintar, A. Efficient catalytic abatement of greenhouse gases: Methane reforming with CO₂ using a novel and thermally stable Rh-CeO₂ catalyst. *Int. J. Hydrogen Energy* **2012**, *37*, 2699–2707. [[CrossRef](#)]
6. Chen, J.; Yao, C.; Zhao, Y.; Jia, P. Synthesis gas production from dry reforming of methane over Ce_{0.75}Zr_{0.25}O₂-supported Ru catalysts. *Int. J. Hydrogen Energy* **2010**, *35*, 1630–1642. [[CrossRef](#)]
7. Gaur, S.; Haynes, D.J.; Spivey, J.J. Rh, Ni, and Ca substituted pyrochlore catalysts for dry reforming of methane. *Appl. Catal. A* **2011**, *403*, 142–151. [[CrossRef](#)]
8. Gamba, O.; Moreno, S.; Molina, R. Catalytic performance of Ni-Pr supported on delaminated clay in the dry reforming of methane. *Int. J. Hydrog. Energy* **2011**, *36*, 1540–1550. [[CrossRef](#)]
9. Gonzalez-Delacruz, V.M.; Perenguez, R.; Ternero, F.; Holgado, J.P.; Caballero, A. In situ XAS study of synergic effects on Ni-Co/ ZrO₂ methane reforming catalysts. *J. Phys. Chem. C* **2012**, *116*, 2919–2926. [[CrossRef](#)]
10. Wang, N.; Chu, W.; Zhang, T.; Zhao, X.S. Manganese promoting effects on the Co-Ce-Zr-O_x nano catalysts for methane dry reforming with carbon dioxide to hydrogen and carbon monoxide. *Chem. Eng. J.* **2011**, *170*, 457–463. [[CrossRef](#)]
11. Djokovic, P.; Crniveca, I.O.; Erjaveca, B.; Pintara, A. Influence of active metal loading and oxygen mobility on coke-free dry reforming of Ni-Co bimetallic catalysts. *Appl. Catal. B Environ.* **2012**, *125*, 259–270.
12. Al-Doghachi, F.A. Effects of Platinum and Palladium Metals on Ni/Mg_{1-x}Zr_xO Catalysts in the CO₂ Reforming of Methane. *Bull. Chem. React. Eng. Catal.* **2018**, *13*, 295–310. [[CrossRef](#)]
13. Grange, P. Catalytic Hydrodesulfurization. *Catal. Rev. Sci. Eng.* **1980**, *21*, 135–181. [[CrossRef](#)]
14. Devaraja, P.B.; Avadhani, D.N.; Prashant, S.C.; Nagabhushana, H.; Sharma, S.C.; Nagabhushana, B.M.; Nagaswarupa, H.P. Synthesis, Structural and Luminescence Studies of Magnesium Oxide Nanopowder. *Spectrochim. Acta Part A Mol. Biomol. Spectrosc.* **2014**, *118*, 847–851.
15. Hidalgo, C.; Jalila, S.; Alberto, M.; Said, S. XPS Evidence for Structure—Performance Relationship in Selective Hydrogenation of Croton aldehyde to Crotyl Alcohol on Platinum Systems Supported on Natural Phosphates. *J. Colloid Interface Sci.* **2012**, *382*, 67–73. [[CrossRef](#)] [[PubMed](#)]
16. Mahoney, E.G.; Pusel, J.; Stagg, W.S.; Faraji, S. The Effects of Pt Addition to Supported Ni Catalysts on Dry (CO₂) Reforming of Methane to Syngas. *J. CO₂ Util.* **2014**, *6*, 40–44. [[CrossRef](#)]
17. Bao, Z.; Lu, Y.; Han, J.; Li, Y.; Yu, F. Highly Active and Stable Ni-based Bimodal Pore Catalyst for Dry Reforming of Methane. *Appl. Catal. A* **2015**, *491*, 116–126. [[CrossRef](#)]
18. Roberto, B.S.; Juniora, R.C.; Rabelo, N.S.; Gomes, F.N. Steam reforming of acetic acid over Ni-based catalysts derived from La_{1-x}Ca_xNiO₃ perovskite type oxides. *Fuel* **2019**, *82*, 20081–20312.
19. Al-Doghachi, F.A.; Taufiq-Yap, Y.H. CO₂ Reforming of Methane over Ni/MgO Catalysts Promoted with Zr and La Oxides. *Chem. Sel.* **2018**, *3*, 816–827. [[CrossRef](#)]
20. Djadja, A.; Libs, S.; Kiennemann, A.; Barama, A. Characterization and Activity in Dry Reforming of Methane on Ni,Mg/Al and Ni/MgO Catalysts. *Catal. Today* **2006**, *113*, 194–200. [[CrossRef](#)]
21. Ahmed, W.; Awadallah, A.E.; Aboul, E.A. Ni/CeO₂-Al₂O₃ Catalysts for Methane Thermo-catalytic Decomposition to CO_x-free H₂ Production. *Int. J. Hydrogen Energy* **2016**, *41*, 18484–18493. [[CrossRef](#)]
22. Mojović, Z.; Mentus, S.; Tesic, Z. Introduction of Pt and Pd Nanoclusters in Zeolite Cavities by Thermal Degradation of Acetylacetonates. *Mater. Sci. Forum* **2004**, *453*, 257–262. [[CrossRef](#)]
23. Al-Doghachi, F.A.; Islam, A.; Zainal, Z.; Saiman, M.I.; Embong, Z.; Taufiq-Yap, Y.H. High Coke-Resistance Pt/Mg_{1-x}Ni_xO Catalyst for Dry Reforming of Methane. *PLoS ONE* **2016**, *11*, 145–862. [[CrossRef](#)]
24. Aramouni, N.A.; Zeaiter, J.; Kwapinski, W.; Leahy, J.J.; Ahmad, M.N. Eclectic trimetallic Ni-Co-Ru catalyst for the dry reforming of methane. *Int. J. Hydrog. Energy* **2020**. In Press. [[CrossRef](#)]
25. Kehres, J.; Jakobsen, J.G.; Andreasen, J.W.; Wagner, J.B.; Liu, H.; Molenbroek, A.; Vegge, T. Dynamical Properties of a Ru/MgAl₂O₄ Catalyst During Reduction and Dry Methane Reforming. *J. Phys. Chem.* **2012**, *116*, 21407–21415. [[CrossRef](#)]
26. Al-Doghachi, F.A.; Rashid, U.; Taufiq-Yap, Y.H. Investigation of Ce (III) Promoter Effects on the Tri-metallic Pt,Pd,Ni/MgO Catalyst in Dry-reforming of Methane. *RSC Adv.* **2016**, *6*, 10372–10384. [[CrossRef](#)]
27. Giordano, F.; Trovarelli, A.; Leitenburg, C.; Giona, M.A. Model for the Temperature—Programmed Reduction of Low and High Surface Area Ceria. *Catalysis* **2000**, *193*, 273–282. [[CrossRef](#)]
28. Steinhauer, B.; Kasireddy, M.; Radnik, J.; Martin, A. Development of Ni-Pd Bimetallic Catalysts for the Utilization of Carbon Dioxide and Methane by Dry Reforming. *Appl. Catal. A* **2009**, *366*, 333–341. [[CrossRef](#)]

29. Istadi, I.; Anggoro, D.D.; Amin, N.S.; Ling, D.W. Catalyst deactivation simulation through carbon deposition in carbon dioxide reforming over Ni/CaO-Al₂O₃ catalyst. *Bull. Chem. React. Eng. Catal.* **2011**, *6*, 129–136. [[CrossRef](#)]
30. Zhang, H.; Li, M.; Xiao, P.; Liu, D.; Zou, C.J. Structure and Catalytic Performance of Mg-SBA-15-Supported Nickel Catalysts for CO₂ Reforming of Methane to Syngas. *Chem. Eng. Technol.* **2013**, *36*, 1701–1707.
31. Al-Doghachi, F.A.; Rashid, U.; Zainal, Z.; Saiman, M.I.; Taufiq-Yap, Y.H. Influence of Ce₂O₃ and CeO₂ Promoterson Pd/MgO Catalysts in the Dry-reforming of Methane. *RSC Adv.* **2015**, *5*, 81739–81752. [[CrossRef](#)]
32. Al-Doghachi, F.A.; Islam, A.; Zainal, Z.; Saiman, M.I.; Embong, Z.; Taufiq-Yap, Y.H. Hydrogen Production from Dry-Reforming of Biogas over Pt/Mg_{1-x}Ni_xO Catalysts. *Energy Procedia* **2015**, *79*, 18–25. [[CrossRef](#)]



© 2020 by the authors. Licensee MDPI, Basel, Switzerland. This article is an open access article distributed under the terms and conditions of the Creative Commons Attribution (CC BY) license (<http://creativecommons.org/licenses/by/4.0/>).